TSUNAMI GENERATION BY SUBMARINE MASS FAILURE

PART I : WAVEMAKER MODELS

By Philip Watts[1], and Stéphan T. Grilli[2], Member, ASCE

[1]Applied Fluids Engineering, Private Mail Box #237, 5710 E. 7th Street, Long Beach, CA 90803.
[2]Prof., Dept. of Ocean Engng., Univ. of Rhode Island, Narragansett, RI 02882.

ABSTRACT

Numerical experiments are conducted for two-dimensional model problems of tsunami generation by underwater slides and slumps. These problems consist of semi-ellipses translating down an incline with a prescribed center of mass motion. For each problem, landslide motion is derived as a function of geometric and material parameters. We calculate tsunami amplitudes numerically. Landslide deformation is shown to have negligible effect on these amplitudes. Results from numerical experiments of the model problems are converted into predictive curve fits of characteristic tsunami amplitudes as functions of nondimensional governing parameters. These results are useful for estimating tsunami hazard or for performing case studies. A method is proposed to input free surface displacements, modeled shortly after tsunami generation, into tsunami propagation models, in essence treating submarine mass failures tsunami sources exactly like coseismic displacement tsunami sources.

INTRODUCTION

Submarine mass failures (SMF), or underwater landslides, are synonymous terms that encompass all submerged rock slides, reef failures, and many forms of sediment failure,

slow or fast. SMF classification can be made on the basis of landslide morphology, landslide material, or landslide dynamics, with no systematic preference yet established (Hampton *et al.*, 1996; Turner and Schuster, 1996). We will study tsunami generation by two idealized forms of SMF: underwater slides and underwater slumps. Underwater slides are identified by thin, translational, failures that travel long distances, while underwater slumps are defined to undergo thick, rotational, failures with minimal displacement (Prior and Coleman, 1979; Edgers and Karlsrud, 1982; Schwab *et al.*, 1993).

The amplitude of tsunamis generated by SMF can vary from being imperceptible to dominating local tsunami hazards. In fact, tsunamis generated by SMF appear to be one of the major coastal hazards for moderate earthquakes (e.g., Tappin *et al.,* 1999, 2001). Tsunamis generated by coseismic displacement are usually relatively small for moderate earthquakes, since tsunami amplitude correlates with earthquake moment magnitude. Tsunamis caused by SMF, however, are only limited in amplitude by the SMF vertical displacement (Murty, 1979; Watts, 1998). Because SMF usually occur on the continental slope, such displacements may reach several thousand meters and thereby produce huge tsunamis regardless of earthquake magnitude. Moreover, such tsunamis offer little time for warning due to the proximity of the continental slope to shore (Grilli and Watts, 1999; Watts, 2000).

It is therefore of prime importance for tsunami hazard assessment to quickly and reliably predict SMF tsunami amplitudes as a function of governing geological and geometrical parameters. In particular, such predictions are necessary: (i) to estimate the tsunami hazard of SMF, in an order of magnitude sense; (ii) to increase the accuracy of SMF tsunami case studies and scenarios in those instances where specific marine geology information is present; and (iii) to assess the errors in tsunami amplitude associated with uncertainty in SMF location, shape, or motion. Summaries of tsunamis affecting the United States can be

found in Lander and Lockridge (1989), Lander *et al*. (1993), and Lander (1996). A reasonably complete case study of the 1998 Papua New Guinea tsunami is available from the work of Tappin *et al*. (1999, 2001) and Watts *et al*. (2002).

SMF Tsunami Modeling

Laboratory and analytical studies of water waves generated by SMF have been conducted by Wiegel (1955), Iwasaki (1982), Heinrich (1992), and Watts (1997, 1998, 2000). Two-dimensional (2D) numerical simulations of water waves generated by SMF have been conducted by Iwasaki (1987, 1997) and Harbitz (1992) using linear shallow water wave (LSW) equations, by Verriere and Lenoir (1992) using linearized potential flow equations, by Heinrich (1992) and Assier-Rzadkiewicz *et al*. (1997) using a volume of fluid (VOF) solution of Navier-Stokes (NS) equations, and by Jiang and LeBlond (1992, 1993, 1994), Imamura and Gica (1996) and Fine *et al*. (1998) using nonlinear shallow water wave (NSW) equations with a two-phase flow model.

Grilli and Watts (1999) applied a fully nonlinear potential flow (FNPF) model to water wave generation by underwater landslides following the wavemaker formalism introduced by Watts (1998) to specify underwater landslide geometry and kinematics. Grilli *et al*. (1989), Grilli and Svendsen (1990), and Grilli and Subramanya (1996) incrementally developed and validated this efficient 2D-FNPF model, in which governing equations are solved by a higher-order Boundary Element Method (BEM). Time integration is based on second-order explicit Taylor series expansions of the free surface position and the velocity potential. The model reproduced laboratory experiments for solitary wave shoaling and breaking on a slope to within a few percent (Grilli *et al*., 1994, 1998) and various other long-wave runup benchmark problems (Yeh *et al*., 1996). [The interested reader can also compare the experimental work of Li and Raichlen (1998) with the numerical results of

Grilli *et al*. (1998).] Grilli and Watts (1999) performed a sensitivity analysis for one underwater landslide scenario. More recently, Watts *et al*. (2000) validated the model with experimental landslide tsunami results. This extensive work gives us confidence to use BEM simulations as a numerical wave tank (Grilli and Watts, 2001).

Here, we calculate tsunami amplitudes generated by various SMF shapes and motions using the 2D-FNPF model described above. The tsunami amplitudes will be represented by analytical curve fits as a function of (nondimensional) governing parameters. Curve fits can turn large amounts of numerical simulation results into predictive equations that can be used to make quick and reliable estimates of tsunami amplitude in many situations. Thus, a modest number of numerical simulations can provide almost unlimited interpolation of SMF tsunami amplitudes. Moreover, the errors inherent in such estimates are available by repeated evaluation, or by taking partial derivatives, of the curve fits themselves. We are aware of only three previous predictive tsunami amplitude equations with either sloping inclines or accelerating landslides. One of two semi-empirical equations proposed by Striem and Miloh (1976) is reproduced by Murty (1979). The theoretical equation of Pelinovsky and Poplavsky (1996) was shown to produce reasonable tsunami amplitude predictions by Watts *et al*. (2000). Last of all, the works of Grilli and Watts (1999) and Goldfinger *et al*. (2000) provide predictive equations that are precursors to the work presented here.

As evidenced by our earlier results, complete fluid dynamic simulations, such as those performed with this FNPF model, are key to the accurate modeling of tsunami landslides. Complete simulations capture both horizontal and vertical water accelerations generated by an accelerating SMF (Grilli and Watts, 1999). Furthermore, free surface and moving boundary conditions are fully nonlinear in the model. Comparisons between numerical simulations and experimental results have consistently demonstrated the benefits of

simulating exact field equations and boundary conditions over simpler but approximate depth-averaged LSW or NSW equations (Yeh *et al.*, 1996; Watts *et al.*, 2000). Finally, the assumption of inviscid, irrotational, flows is justified for non-breaking wave propagation, and a VOF solution of NS equations seems unnecessary given the viscosity of water. These considerations justify the proposed modeling approach.

Model Problems

Numerical simulations of SMF in the 2D-FNPF model may reproduce laboratory experiments or duplicate given historical events, as in some of the references cited above. Here, for the purpose of deriving predictive equations of tsunami amplitudes, we simulate idealized "model problems" of tsunami generation by SMF. Given that an accurate source depiction is rarely available for SMF tsunamis, we specify an approximate SMF geometry, such as a semi-ellipse in the vertical plane resting on a straight incline, with angle θ from horizontal (Fig. 1). The semi-ellipse has a maximum thickness T along the minor semi-axis, a total length b along the major axis, and an initial vertical submergence d at the middle of the landslide. Our 2D model problem is identical to that studied by Grilli and Watts (1999). The landslide has a width w and is assumed to be homogenous in the width direction, with $w/b \gg 1$, justifying a 2D approximation. Hence, the landslide volume is $V = \pi bTw/4$, and its maximum cross section perpendicular to the direction of motion (parallel to the incline) is $A = Tw$. A numerical wave gage is located at x_g (see Fig. 1) to record a characteristic tsunami elevation above the maximum initial SMF thickness. Using the wavemaker formalism of Watts (1998), we derive the center of mass motions along the incline as a function of the governing parameters in our model problem. Underwater slides and slumps are distinguished solely by their center of mass motion along the straight incline. Initially, we assume negligible SMF deformation, although we are free to test this assumption. We believe that numerical simulations need to first accurately reproduce the

SMF initial acceleration before introducing and interpreting additional effects of deformation and changing bathymetry. The largest source of error in the numerical simulations is a ±2% discretization error in tsunami amplitude.

Scaling of Tsunami Features

Watts (1997) documented a narrow-banded frequency spectrum from wave gage measurements made during landslide tsunami experiments. This indicates that there is a characteristic period for landslide tsunamis. Whenever the landslide characteristic time of motion t_o is much smaller than the tsunami propagation time $b/\sqrt{gd}$ (where g is the acceleration of gravity), this period is proportional to t_o, regardless of SMF material (Watts, 1998, 2000). [For tsunamis generated by coseismic displacement, Hammack (1973) showed the characteristic period is proportional to $b/\sqrt{gd}$]. The characteristic wavelength of a landslide tsunami easily follows as

$$\lambda_o = t_o \sqrt{gd} \tag{1}$$

where d is a rough approximation of the local bathymetry. To understand the origin of the narrow spectra, we note that linear wavemaker theory predicts that waves with wavelength $\lambda < d$ will be filtered out of tsunami generation (Dean and Dalrymple, 1991). We also note that the leading elevation (or Airy) wave has effectively infinite wavelength (Mei, 1983). A strong spectral peak can be expected whenever Eq. (1) predicts a ratio $\lambda_o/d > 1$ which is between these two bounds. For the work of Watts (1997), one finds a typical ratio $\lambda_o/d \approx 3$ for most of the solid block experiments reported. Hence, one should verify that SMF motion is slower than tsunami propagation and that the ratio $\lambda_o/d > 1$ before using the equations we provide here.

In the work of Wiegel (1955) and Watts (2000), landslide tsunami amplitudes decayed with distance to the 1/3 power along a constant depth channel. This decay rate corresponds to the asymptotic behavior of a volumetric source, even though underwater landslides displace no net mass (Mei, 1983). This appears paradoxical because landslide tsunami generation appears to behave more like a doublet (i.e., piling water ahead of the landslide and pulling it down behind the landslide, as in Fig. 1) than a source. However, in order to behave like a true doublet, landslide velocity would have to be fast relative to tsunami propagation speed (Batchelor, 1967). Watts (1998, 2000) showed that most underwater landslides generate tsunamis with periods several times slower than the duration of tsunami propagation across the generation region. Given this fact, the resulting tsunami energy becomes highly directed along the axis of landslide failure (Ben-Menahem and Rosenman, 1972). Iwasaki (1997) documented this strong directivity of landslide tsunami energy. The tsunami behaves as two distinct sources: an elevation source propagating ahead in the direction of motion, and a depression source situated above the landslide, the two sources being separated by a distance proportional to λ_o. The sum of these two sources has a zero mass flux, the sources being equal in strength, yet opposite in polarity. Eq. (1) shows that shorter landslide motion would bring these two sources closer together, form the anticipated doublet, and result in more rapid far-field tsunami amplitude decay rates.

Because our model problems are 2D, we propose criteria for 2D tsunami generation in a three-dimensional basin (Grilli and Watts, 2001). These criteria involve the characteristic wavelength given in (1). In addition to $w \gg b$, as introduced before, SMF must have a width w much greater than the local water depth as well as the characteristic wavelength

$$w \gg d \ , \ w \gg \lambda_o \tag{2a,b}$$

in order to generate a 2D tsunami that is only mildly affected by the third spatial dimension during times $t < t_o$. Depth and wavelength are length scales that represent landslide geometry and dynamics, respectively. The characteristic wavelength is also a measure of lateral tsunami propagation during tsunami generation. Lateral propagation along the landslide width can reduce tsunami amplitude. This fact provides strong motivation for three-dimensional work on tsunami generation (Grilli and Watts, 2001), which we defer for now in favor of more complete 2D analyses.

WAVEMAKER MODELS

We convert morphological descriptions of SMF into two idealized descriptions based on dynamical considerations. Our two choices, underwater slides and underwater slumps, then become convenient end members for the general range of possible SMF motions. The (almost) frictionless motion of a slide yields a terminal velocity that is essentially limited by fluid dynamic drag and the length of the incline. By the time the slide comes to rest within some oceanic deep, considerable deformation may have occurred, or a turbidity current may have formed (Lee *et al.*, 1991). On the other hand, the rotation of a cohesive slump is retarded by significant basal friction that can keep fluid dynamic drag from reaching important scales. Whereas a slump may not travel very far before coming to rest, it may break into distinct blocks that experience significant relative motion (Lee *et al.*, 1991). Tsunami amplitudes above slides or slumps scale with characteristics of center of mass motion (Watts, 1998, 2000).

Slide Center of Mass Motion

We model an underwater slide as a rigid body moving along a straight incline (Fig. 1), with center of mass motion *s(t)* parallel to the incline subject to a balance of forces. Dobry *et al.*

(1982) and Seed *et al*. (1988) show that sand and silt can experience a drop in shear strength by up to an order of magnitude during slope failure, thereby justifying neglect of a frictional force. Hence, balancing inertial, added mass, gravitational, buoyancy, and fluid dynamic drag forces, we find

$$(\rho_b + C_m\,\rho_w)\,V\,\frac{d^2s}{dt^2} \;\approx\; (\rho_b - \rho_w)\,V\,g\,\sin\theta \;-\; \frac{1}{2}C_d\,\rho_w\,A\left(\frac{ds}{dt}\right)^2 \tag{3}$$

where ρ_b is the bulk slide density, ρ_w is the water density, C_m is the added mass coefficient, and C_d is the drag coefficient. The differential equation (3) is still dissipative, despite neglect of Coulomb friction, which becomes necessary only to halt sliding in a finite time (Watts, 1997). Assuming $s = 0$, $ds/dt = 0$, and $d^2s/d^2t = a_0$ at time $t = 0$ as well as a terminal velocity $ds/dt \approx u_t$ and acceleration $d^2s/d^2t \approx 0$ at large times, Eq. (3) leads to

$$\frac{a_o}{g} \;=\; \frac{\gamma - 1}{\gamma + C_m}\sin\theta \tag{4}$$

$$\frac{u_t}{\sqrt{gb}} \;=\; \sqrt{\frac{\pi(\gamma - 1)}{2C_d}\sin\theta} \tag{5}$$

where $\gamma = \rho_b/\rho_w$ is the specific density. Using definitions (4) and (5), the exact solution of Eq. (3) becomes

$$s \;=\; s_O \ln\left[\cosh\left(\frac{t}{t_o}\right)\right] \tag{6}$$

$$s_O \;=\; \frac{u_t^{\,2}}{a_o} \text{ and } t_O \;=\; \frac{u_t}{a_o} \tag{7a,b}$$

in which s_O denotes a characteristic distance of motion. Eq. (6) is a common analytical solution for free bodies subject to gravity and form drag at high Reynolds numbers

(Pelinovsky and Poplavsky, 1996; Watts, 1997). The form of the solution (6) is unchanged if Coulomb friction is added to (3) and can be represented exactly by adopting an effective slope when calculating slide motion such that $\sin \theta_{eff} = \sin \theta - C_n \cos \theta$, where C_n is the Coulomb friction coefficient. The first term in the Taylor series expansion of (6) about $t = 0$ is $s(t) \approx a_o t^2/2$, as required for a body accelerating from a state of rest. Eqs. (7) shows that a unique characteristic distance and time exist for each underwater slide. Watts (1997) demonstrated that the center of mass motion of deforming slides could also be accurately described by (6), until at least $t \approx t_o$. Hence, changes in effective dynamical coefficients brought on by landslide deformation do not noticeably alter center of mass motion. The center of mass motion at later times becomes influenced by particle effects, including the bulk rotation of the landslide (Watts, 1997).

An appropriate added mass coefficient for Eq. (4) can be selected as $C_m \approx 1$, similar to that of a circular cylinder (Sarpkaya and Isaacson, 1981; Watts, 2000). An appropriate drag coefficient can be selected as $C_d \approx 1$, which is also that of a circular cylinder (Batchelor, 1967; Watts, 1998). For any specified values of γ, C_m, and C_d, we find

$$a_o \sim \mathrm{g} \sin \theta \tag{8a}$$

$$u_t \sim \sqrt{bg \sin \theta} \tag{8b}$$

$$s_o \sim \mathrm{b} \tag{8c}$$

$$t_o \sim \sqrt{b / g \sin \theta} \tag{8d}$$

$$\lambda_o \sim \sqrt{bd / \sin \theta} \tag{8e}$$

where the dependence of center of mass motion on slide length and incline angle is made explicit. Center of mass motion depends on the slide length, as opposed to other measures of landslide size.

Slump Center of Mass Motion

We model an underwater slump as a rigid body moving an angle ϕ along a circular arc (failure plane) subject to external moments from added mass, buoyancy, gravity, and shear stress summed over the failure plane (Fig. 1). The influence of fluid dynamic drag and angular nonlinearity on center of mass motion are often negligible and can be evaluated from the exact solution given by Nayfeh and Mook (1979). Hence, we neglect the drag force and invoke the small angle approximation, $\sin\phi \approx \phi$, to find the linearized differential equation

$$R\,(\rho_b + C_m\,\rho_w)\,V\,\frac{d^2\phi}{dt^2} \approx -\,(\rho_b - \rho_w)\,V\,g\,\phi + A\,S_u \tag{9}$$

describing the slump angular motion, where R is the radius from the slump center of rotation C to the center of mass, $A = b\,w$ is the area of the failure plane projected on the slope, and the shear strength S_u along the failure plane is assumed to remain constant during motion (Bardet, 1997). The solution of Eq. (9) provides $\phi(t)$, which is the motion of a frictional pendulum. Multiplying this solution by the radius of curvature R gives the slump tangential motion along the chosen failure arc

$$s(t) = s_o\left[1 - \cos\left(\frac{t}{t_o}\right)\right] \tag{10}$$

with the characteristic distance of motion given by

$$\frac{s_o}{R} = \frac{(\phi_f - \phi_i)}{2} = \frac{4S_u}{\pi T g(\rho_b - \rho_w)} \tag{11}$$

where ϕ_i and ϕ_f are the initial and final center of mass angles in radians, respectively; and the characteristic time of motion is

$$t_o \sqrt{\frac{g}{R}} = \sqrt{\frac{\gamma + C_m}{\gamma - 1}} \tag{12}$$

in accordance with the period of pendular motion. Once again, we assumed that no motion existed at time $t = 0$. The initial acceleration is $d^2s/d^2t = a_o = s_o/t_o^2$, and the slump comes to a halt at $s(\pi t_o) = 2s_o$. The first term in the Taylor series expansion of Eq. (10) about $t = 0$ is also $s(t) \approx a_o t^2/2$, although the physical parameters that determine the initial acceleration differ from those of a slide. Due to linearization, neglect of fluid dynamic drag, and the assumption of a circular failure plan, the slump motion describe by Eq. (10) must be considered as approximate.

Eq. (10) also appears in the form $s/s_O = f(t/t_O)$, with a unique characteristic distance s_O and characteristic time t_O of slump motion. The value of s_O in Eq. (11) may be fixed by observations of slump center of mass motion, yielding information on a characteristic shear strength S_u along the failure plane. The fact that the characteristic distance of motion is proportional to shear strength S_u raises an apparent paradox that we resolve in Part II of this work. Because Eq. (12) is insensitive to specific gravity, observations of tsunami period t_O suffice to estimate a radius of curvature R and bolster (or refute) classification of a SMF as an underwater slump. We note that Eq. (10) produces a maximum velocity $u_{\max} = s_O/t_O$ at the middle of slump motion, $t = \pi t_O/2$, before returning to rest at the end of motion. For a slump, it is easier to construct the maximum velocity and initial acceleration from the characteristic distance and time than the other way around. For specified values of γ and C_m, we find the simplified relationships

$$a_o \sim g\,\Delta\phi \tag{13a}$$

$$u_{\max} \sim \Delta\phi\,\sqrt{Rg} \tag{13b}$$

$$s_o \sim R\,\Delta\phi \tag{13c}$$

$$t_o \sim \sqrt{R/g} \tag{13d}$$

$$\lambda_o \sim \sqrt{Rd} \tag{13e}$$

where $\Delta\phi = \phi_f - \phi_i$. Center of mass motion depends on the radius of curvature, and not on any explicit measure of slump size, a well-known property of a pendulum. While Eq. (10) applies strictly to translation along a circular arc, we will apply it in our model problem to translation along a straight incline. The error incurred by this approximation is roughly $0.5R\,\Delta\phi^2$, which is negligible in most applications given the limited angular displacement of slumps. For example, we estimate the maximum spatial error to be around 5% of the maximum slump thickness T in the case of the 1998 Papua New Guinea slump.

NONDIMENSIONAL FRAMEWORK

We consider the nondimensional framework of a characteristic tsunami amplitude η generated by an underwater slide. Following the nondimensional technique established by Hammack (1973) and extended by Watts (1998), any chosen near-field tsunami amplitude is an unknown function of the six nondimensional numbers

$$\frac{\eta}{b} = F\left(\frac{d}{b}, \frac{T}{b}, \theta, \gamma, C_m, C_d\right) \tag{14}$$

where, according to (8), the slide length b is an appropriate near-field length scale. Watts (1998) showed that the specific density, added mass coefficient, and drag coefficient in (14) can be formally replaced by the characteristic distance s_o and characteristic time t_o of slide motion, provided the center of mass motion has the form $s/s_o = f(t/t_o)$. This change in

perspective substitutes derived quantities, representing landslide motion, as proxies for primitive quantities that determine this motion. The result is a reduction from six to five nondimensional numbers

$$\frac{\eta}{s_o \sin\theta} = \frac{1}{Ha_o} \mathrm{G}\left(\frac{d}{b}, \frac{T}{b}, \theta, Sg, Ha_o \right) \tag{15}$$

$$Sg = s_o \sin\theta \ / \ \mathrm{d} \ \text{ and } \ Ha_o \approx t_o \sqrt{gd} \ / \ b \tag{16}$$

where Sg is the Submergence number and Ha_o is the Hammack number. Underwater slumps require a modest extension of Eqs. (14) to (16) to account for the additional geometrical quantities $\Delta\phi$ and R/b. We note here that Synolakis (1986) also introduced two dynamical quantities, related to the Hammack and Submergence numbers, in order to describe long wave generation by a piston wavemaker and subsequent run-up along a plane slope. These are the Generation number $S/\tau\sqrt{gd}$ and a nondimensional wavemaker time $\tau\sqrt{g/d}$, where S is a characteristic piston stroke, τ is a characteristic duration of piston motion, and d is the water depth in a constant depth channel. The functional form put forth by Synolakis (1986) to describe long wave run-up is almost identical to Eq. (15). Similar geometries and simple motions lead to nondimensional quantities like those in Eq. (15).

The nondimensional Submergence number Sg is the ratio of the vertical length scale of landslide motion to the initial landslide submergence. [Landslide tsunamis behaving as linear waves do not depend on Sg, which reduces Eq. (15) by one independent quantity.] The nondimensional Hammack number Ha_o is the ratio of the time scale of landslide motion to the time it takes long waves to propagate over the generation region. [The approximate Ha_o in (16), resulting from assuming a uniform depth d above the landslide, is accurate to within about ±20% for the numerical simulations considered here. The exact value of the Hammack number integrates long wave propagation over a sloping bottom

(Grilli and Watts, 1999).] Small Hammack numbers, $Ha_o \ll 1$, imply tsunami generation by rapid displacement, such as coseismic displacement during an earthquake (Hammack, 1973), whereas large Hammack numbers, $Ha_o \gg 1$, imply slow tsunami generation by an accelerating body such as a SMF (Watts, 1998). Thus, most SMF have Hammack numbers $Ha_o > 1$ and generate waves primarily by acceleration.

SIMULATION RESULTS

We begin this section by demonstrating the differences between tsunamis generated by underwater slides and slumps. Then the role of landslide deformation in tsunami generation will be shown to be negligible under certain circumstances. These results justify the model problem employed in this work. We present the methodology developed to reduce and to curve fit the model problem results, with specific attention given to reference conditions. The 2D tsunami amplitude prediction are given along with some cautions about the appropriate use of the curve fits.

Mass Failure Motion

The center of mass motion of a slide is significantly different from that of a slump, and so are the tsunamis generated by these SMF. To make this point clearly, we compare tsunami generation by a slide with that of a slump given identical shape and density. The chosen parameters are $\gamma = 1.85$, $b = 5$ km, $T = 450$ m, $d = 1.2$ km, $\theta = 12^\circ$, $R = 21$ km, and $\Delta\phi = 0.29$, where the last two parameters only apply to the slump. Although some parameters have realistic values, this example is not meant to represent any actual SMF. Using Eqs. (4), (5) and (7), the slide motion is described by Eq. (6) with $s_o = 22$ km and $t_o = 192$ s. Using Eqs. (11) and (12), the slump motion is described by Eq. (10) with $s_o = 3$ km and $t_o = 85$ s. Fig. 2 compares the two center of mass motions. As expected, the slide achieves a

terminal velocity while the slump comes to rest at time $t = \pi t_o$. Despite a large radius of curvature, the duration of slump acceleration is visibly shorter and the maximum slump velocity considerably smaller than the corresponding values for the slide. Fig. 3 shows computed surface elevations at $x = x_g$ above the initial landslide position as shown on Fig. 1. The maximum tsunami trough (or "characteristic") amplitude generated by the underwater slide is four times that of the underwater slump, despite having similar initial accelerations ($a_o = 0.61$ m/s^2 *versus* $a_o = 0.42$ m/s^2, respectively). This is not surprising because: i) the duration of acceleration is proportional to t_o and therefore lasts about twice as long for the slide, ii) the landslide displacement near $t = 0$ goes as time squared, and iii) the tsunami amplitude scales foremost with SMF displacement $s_{o,}$ as shown in Eq. (15). These three facts result in a four-fold increase in tsunami amplitude in favor of the slide. The slide wavelength appears to be about double that of the slump as predicted by Eq. (1).

Mass Failure Deformation

Watts (1997) found experimentally that the primary mode of landslide deformation is through extension parallel to the incline. Watts *et al*. (2000) found the same result for numerical simulations of deformable landslides performed with the model of Imamura and Imteaz (1995). For both experimental and numerical results, the rate of extension was constant (i.e., landslide length grew linearly in time), following an initial transient. The maximum landslide thickness T remained more or less constant over time. Therefore, self-similar landslide deformation can be described by a constant rate of extension Γ, with dimension of inverse time.

To assess the effect of SMF deformation in our numerical simulations of tsunamis features, we specified the landslide semi-ellipse length along the major axis as

$$b(t) = b_o \left\{ 1 + \Gamma t \left[1 - \exp(-K t) \right] \right\} \tag{17}$$

where $K \leq a_o/b_o\Gamma$ is chosen to keep the uppermost portion of the landslide from traveling uphill. [If $K > a_o/b_o\Gamma$, there is an initial transient for which the center of mass velocity downhill $a_o t$ is less than the nominal velocity of extension uphill $b_o\Gamma/2$. When $K = a_o/b_o\Gamma$, the top of the landslide remains immobile during part of the transient, as observed in the experimental work of Watts (1997). We also note that the corresponding expression for K in Watts *et al*. (2000) contains a typo.] Beyond the initial transient, landslide length $b(t)$ in (17) increases linearly in time.

We begin our investigation by determining a reasonable rate of extension for underwater landslides. We invert (17) at large times, to estimate a maximum rate of extension

$$\Gamma_{max} \approx \frac{1}{t} \left[\frac{b}{b_o} - 1 \right] \tag{18}$$

where we need to relate observed landslide extension with some measure of the duration of landslide motion. To do this, we examined underwater landslide records for rough indications of total landslide extension and distance traveled (Prior and Coleman, 1979; Edgers and Karlsrud, 1982; Schwab *et al*., 1993; Hampton et al., 1996). We found indications that $b \approx 3b_o$ and $s \approx 2s_o$ for some highly deformed underwater slide scars and deposits, events for which the rate of deformation can be presumed large. We use Eq. (6) to calculate an associated time $t \approx 3t_o$ and substitute these estimates into Eq. (18), along with the expression for t_o from Eq. (8d) (with $\gamma = 1.85$, $C_M = C_d = 1$), to find

$$\Gamma_{max} \sqrt{\frac{b_o}{g}} \approx \frac{\sqrt{\sin\theta}}{6} \tag{19}$$

which satisfies $\Gamma_{max} \sqrt{b_o / g} < 0.1$ for most slides. In general, we predict from Eq. (18) that $\Gamma_{max} t_o = 2/3$, or that landslides can extend up to 66% during their characteristic time of motion. Eq. (19) reproduces the quantitative values of landslide extension observed by Watts (1997) in laboratory experiments of deforming granular landslides with $\gamma \approx 1.85$. This experimental work depicted granular landslides with $b_o \approx 0.1$ m doubling in length over the distance s_o along an incline angle $\theta = 45°$. We calculate from Eq. (4) that $s = s_o$ corresponds to $t = 1.66\ t_o$ and from Eqs. (18) and (19) the ratio $b/b_o \approx 2.1$ as observed. Watts (1997) found that denser materials deform more rapidly, a result that can be reproduced by using Eqs. (4) and (5) in place of Eq. (8d) when deriving Eq. (19).

However, tsunami amplitudes of deforming landslides were consistently observed smaller than otherwise identical solid block experiments. We believe that tsunami amplitudes were diminished because of significant flow through the granular landslides. The tsunami amplitude results of Watts (1997) therefore represent experimental artifacts and should not be applied to real events. Most underwater landslides composed of natural sediment would not have significant flow through the failed mass until much later times if a transition to a turbidity current occurs. For tsunamigenic SMF, bulk failure results from internal changes in pore water pressure and crack propagation through sediment rather than flow through the landslide.

To investigate the impact of landslide deformation on tsunami features, we return to the previous underwater slide example where $\theta = 12°$ and $b_o = 5$ km. We compute from Eq. (19) a maximum rate of extension $\Gamma_{max} = 0.00337\ s^{-1}$ and perform the numerical simulation with a deforming slide geometry governed by Eq. (17), and center of mass

motion described by Eq. (6). As usual, we locate a wave gage above the middle of the initial landslide position at $x = x_g$ and document changes in tsunami features due to deformation. Fig. 4 shows that tsunami features such as the tsunami amplitude and wavelength are almost unaffected by deformation. The initial drop in wave amplitude is slightly faster when deformation is present and then proceeds more slowly at later times, as noted by Watts *et al.* (2000). Overall, landslide deformation appears to have accomplished little more than shifting the wave record to the right (and in this case down) by a small amount. The near-field characteristic tsunami amplitude, defined as the absolute maximum amplitude at x_g, is listed in Table 1 for three different incline angles and three rates of extension three times larger than Γ_{max} provided by Eq. (19). Even for such large rates of extension, we find fairly small differences in characteristic tsunami amplitude, and a complex relationship between rate of extension and characteristic tsunami amplitude. Landslide deformation can either increase or decrease tsunami amplitude. Based on these results, the emphasis of Jiang and LeBlond (1992, 1993, 1994) on landslide deformation appears to be unnecessary. In the absence of reliable marine geology, accurate failure geometry, and detailed sediment rheology, we believe that the influence of landslide deformation on tsunami features can be neglected for most submarine mass failures as a first approximation. Moreover, effects such as changing bathymetry, sediment scouring, or deposition, and bulk landslide dilution may be neglected for many studies of landslide tsunami generation because these effects often become important only at later times. Center of mass motion appears to affect tsunami features much more than landslide deformation.

Tsunami Amplitude Fitting Procedure

We demonstrate the fitting procedure for underwater slides. One is free to choose any characteristic tsunami amplitude for which to construct the functions in Eqs. (14) or (15). Here, we choose the maximum tsunami amplitude above the initial mass failure location at x

$= x_g$ as a characteristic tsunami amplitude (Pelinovsky and Poplavsky, 1996; Watts, 1998, 2000). We assume no SMF deformation and proceed with the primitive nondimensional parameters contained in Eq. (14), the constant dynamical coefficients employed above ($C_m = 1$, $C_d = 1$, $C_n = 0$), and the form of the nondimensional tsunami amplitude given by Eq. (15). [We include the characteristic distance from Eq. (15) because it already captures most of the scaling between landslide motion and tsunami amplitude. We can substitute primitive quantities for s_o at a later time from (8) and (13).] In order to facilitate the curve fitting process, we follow the theoretical analysis of Buckingham (1914) and write the nondimensional characteristic tsunami amplitude of an underwater slide in the separable form

$$\eta' = \frac{\eta}{s_o \sin\theta} = F(\sin\theta)\, G\left(\frac{T}{T_{ref}}\right) H\left(\frac{d}{d_{ref}}\right) \tag{20}$$

where $T_{ref} = b \sin\theta$ is a reference thickness, $d_{ref} = 0.2b \sin\theta$ is a reference depth, and the specific density has a consant reference value $\gamma_{ref} = 1.85$. [Note that for slumps the radius of curvature has $R_{ref} = 2b$, and the angular displacement has $\Delta\phi_{ref} = 0.3491$ radians.]

The reference values were selected to turn the primitive nondimensional quantities either into constants, or into functions of incline angle. We define the functions G and H with unit values for the reference thickness and reference depth, respectively. In fact, the identities $G(1) \equiv 1$ and $H(1) \equiv 1$ with nondimensional arguments explain the desire for reference values in the first place. An underwater slide corresponding to all of the reference values produces a reference tsunami amplitude $\eta_{ref} = F\, s_o \sin\theta$ that is solely a function of the incline angle. This process is illustrated in Fig. 5, where the function F is found by curve fitting six numerical experiments, for which $T = T_{ref}$ and $d = d_{ref}$ for different incline angles (Cases 1 to 6 in Table 2). We find that F increases with decreasing incline angle, perhaps due to increased tsunami generation efficiency for nearly horizontal landslides. If

the separable form proposed for Eq. (20) is truly valid, then the functional relation depicted in Fig. 5 is unique and universal over the parameter range studied.

In Fig. 6, thirteen simulations that cover a wide range of slide length and incline angles, while satisfying $T = T_{ref}$ (Cases 7 to 16 in Table 2), are seen to produce nondimensional characteristic amplitudes η/η_{ref} that collapse onto a single curve $H(d/d_{ref})$, which is readily fit by a power function. As could be expected, we see that tsunami amplitude drops dramatically as the initial submergence increases. The submergence number *Sg* becomes singular when the initial submergence *d* vanishes, a singularity that appears to be reflected in Fig. 6. Three distinct simulations anchor the curve fit to the point (1,1) in such a manner that H does not impact the numerical value of F. Similarly, Fig. 7 yields a function $G(T/T_{ref})$ based on thirteen additional numerical experiments satisfying $d = d_{ref}$ (Cases 17 to 26 in Table 2), which demonstrate that tsunami amplitudes are nearly proportional to landslide thickness. The collapse depicted in Figs. 6 and 7 is *a posteriori* validation of the functional form of Eq. (20) given the wide range of parameters involved in these numerical experiments.

Tsunami Amplitude Curve Fits

We performed 32 underwater slide (Table 2) and 12 underwater slump numerical experiments (Table 3), the latter being reduced in the same manner presented above. We present curve fits of numerical results in the form of Eq. (20) here. We employ the subscript "2d" to remind the reader that our curve fits apply to underwater landslides that satisfy the 2D criteria (2). The equation predicting tsunami amplitude for translational slides that experience negligible basal friction but significant fluid dynamic drag is

$$\eta_{2d} \approx s_o \left(0.04772 - 0.03559 \sin\theta + 0.00813 (\sin\theta)^2 \right)$$

$$\left(\frac{T}{b}\right)\left(\frac{b \sin\theta}{d}\right)^{1.25} 1.18(1 - \exp[-2.2(\gamma - 1)]) \qquad (21)$$

where s_o defines the slide motion in Eq. (6). Eq. (21) has an intrinsic amplitude accuracy of ±3.4% at one standard deviation, provided slide shape and motion are exact. This intrinsic accuracy is very similar to the ±2% discretization error in the numerical simulations. The last term in Eq. (21) is unity when the specific density matches the reference value $\gamma_{ref} = 1.85$, and represents the effect of specific density, obtained from results of Cases 27 to 32 in Table 2. These cases were left out of the data in Figs. 5-7. The constraints to Eq. (21), based on the data in Table 2, are that $\theta < 30°$, $T/b < 0.2$, $1.46 < \gamma < 2.93$, and $d/b > 0.06$. The power $(d/b)^{-1.25}$ found from Fig. 6 is accurate to within 0.0039 with $R^2 = 0.9983$. We therefore find during tsunami generation the same exponent as in Green's Law, which applies to tsunami run-up along an inclined plane (Synolakis, 1986). By way of contrast, Pelinovsky and Poplavsky (1996) found the power d^{-1} for tsunami generation in a constant depth channel. It appears that the similar geometries between tsunami generation and tsunami run-up on a sloping incline result in similar scaling with depth. The power of 1.00 for T/b found from Fig. 7 is accurate to within 0.053 with $R^2 = 0.9993$. The second-order polynomial curve fit as a function of $\sin\theta$ from Fig. 5 has $R^2 = 0.9999$. The 1.25 power of the other sine function in (21) is a combination of the left hand side of Eq. (20) with substitution of the reference values T_{ref} and d_{ref}. The specific density function is the least accurate of the curve fits, with $R^2 = 0.9885$. We introduce Eq. (8c) into Eq. (21) with $\gamma = 1.85$ to obtain

$$\eta_{2d} \approx 0.2139\, T \left(1 - 0.7458 \sin\theta + 0.1704 (\sin\theta)^2\right)\left(\frac{b \sin\theta}{d}\right)^{1.25} \qquad (22)$$

where the maximum thickness provides the necessary dimension of length. When the volume per unit width of the slide $\pi Tb/4$ is divided out of Eq. (22), we find that the tsunami amplitude is a strong function of incline angle θ, a mild function of slide length b, and a strong function of initial submergence d. We conclude that underwater slide tsunami amplitude is primarily a function of landslide volume, incline angle, and initial submergence. Fig. 8 compares the simulated amplitude η'_s to the predicted amplitude η'_p found from Eq. (21) for the 32 numerical experiments in Table 2, which covers the entire range of validity of the curve fits. The agreement is very good, thereby demonstrating the predictive ability of the curve fitting procedure within the given range of validity. We note that the tsunami amplitude accuracy is uniform in Fig. 8 because the discretization error in the model is proportional to tsunami amplitude.

Similarly, we find an equation predicting a 2D tsunami amplitude for rotational slumps that experience strong basal friction but minimal fluid dynamic drag

$$\eta_{2d} \approx s_o \, 0.1309 \, (\sin\theta)^{0.22} \left(\frac{T}{b} \right) \left(\frac{b}{d} \right)^{1.25} \left(\frac{b}{R} \right)^{0.63}$$

$$\Delta\phi^{0.39} \left(1.4662 - 0.3454 \, (\gamma - 1) \right) (\gamma - 1) \qquad (23)$$

where s_o defines the slump motion in (10). Eq. (23) has an intrinsic amplitude accuracy of ±2.2% at one standard deviation if the slump shape and motion are exact. The constraints to Eq. (23) are that $\theta < 30°$, $\Delta\phi < 0.53$, $T/b < 0.2$, $1 < R/b < 2$, $1.46 < \gamma < 2.93$, and $d/b > 0.06$. The last term in Eq. (23) is unity when the specific density matches the reference value. The power -0.63 for R/b is accurate to within about 0.039, with $R^2 = 0.9989$. The power -0.78 for $\sin\theta$ is accurate to within about 0.077, with $R^2 = 0.9983$. The 0.22 power of the sine function in (23) is a combination of the left hand side of Eq. (20) with the curve fit power -0.78. It appears that another functional form could be more accurate for these

last two curve fits, but we favor simplicity. The power 0.39 for $\Delta\phi$ is accurate to within 0.005, with $R^2 = 0.9999$. We introduce Eq. (14c) into Eq. (23) with $\gamma = 1.85$ to obtain

$$\eta_{2d} \approx 0.0654\, T\, (\sin\theta)^{0.22}\, (b/d)^{1.25}\, (R/b)^{0.37}\, \Delta\phi^{1.39} \tag{24}$$

where the relative importance of angular displacement and radius of curvature is switched. When the volume per unit width of the slump $\pi Tb/4$ is divided out of Eq. (24), we find that the tsunami amplitude is a mild function of incline angle, a mild function of slump length, a mild function of radius of curvature, a strong function of initial submergence, and a strong function of angular displacement. We conclude that slump tsunami amplitude is primarily a function of landslide volume, initial submergence, and angular displacement.

Appropriate Use of Curve Fits

The analytical curve fits given here have an accuracy that is measured against model problem results. There is no guarantee as to their accuracy for other SMF geometries or motions, which may form the large majority of real events. Specific cautionary notes need to be listed and justified. First of all, a 2D geometry limits applications to wide landslides that satisfy Eqs. (2), and our choice of characteristic tsunami amplitude applies only above the landslide, without consideration of propagation effects. Second, the curve fits imply significant interpolation. In the cases of incline angle and mass failure thickness, most realistic scenarios are covered here and interpolation to zero inclination or thickness is considered highly accurate. On the other hand, the nondimensional ratio $d/b > 0.06$ is needed to avoid wave breaking and other nonlinear phenomena that were not simulated (Watts, 1998). While the limit of vanishing d/b diverges and may introduce inaccuracy, the opposite limit of large d/b can be considered accurate. Last of all, we suggest that all applications of the curve fits be made with estimates of the errors in landslide geometry and

motion tailored to each case study. Repeated application of the curve fits with different inputs (or taking partial derivatives of the amplitude equations) will then yield expected errors in the tsunami features. Hence, the confidence levels can be found for the results.

CONCLUSIONS

While Part I of this work has been largely theoretical, we demonstrate in Part II that our results offer a new and useful understanding of tsunami generation. We explained the relation between a characteristic wavelength and the frequency spectrum of landslide tsunamis. We also explained the far-field behavior of landslide tsunamis, including the strong directivity of energy along the axis of failure. Here, we distinguished between tsunami generation by two types of submarine mass failures: underwater slides, which were the subject of previous papers, and underwater slumps, which represent approximately 50% of all underwater landslides (Schwab *et al*., 1993). Pelinovsky and Poplavsky (1996) and Watts (1997, 1998) derived the center of mass motion of an underwater slide. We derived the center of mass motion of an underwater slump in this work. Previous scaling analyses are reinterpreted and compared based on the two different center of mass motions, specifically the common role of initial acceleration during tsunami generation. We compare tsunami features of underwater slides and slumps for identical density and geometry and find very different amplitudes and wavelengths. We show that reasonable submarine mass failure rates of deformation have little effect on major tsunami features, provided the complete fluid dynamic field equations are solved. Landslide volume and initial depth are two of the most important physical dimensions governing tsunami generation. We conducted accurate numerical experiments of our model problems in order to understand tsunami generation. The main advantage of conducting numerical (instead of laboratory) experiments is that the discretization error can be made as small as necessary to produce

accurate curve fits. Numerical experiments can also cover a much broader range of physical parameters than can be readily performed in a laboratory.

Using curve fits of our numerical experiments, we formulated two-dimensional tsunami amplitude predictions for underwater slides and slumps. The tsunami amplitude accuracy is similar to the ±2% discretization error of the numerical simulations. We explained the procedure of curve fitting the numerical experiments in order to produce accurate predictive tsunami amplitude equations. We also derived the first predictive tsunami amplitude equation for underwater slumps. Our predictive tsunami amplitude equations provide insight into tsunami generation with little computational effort. Repeated evaluation of the curve fits (or taking partial derivatives of the equations) yield tsunami amplitude error estimates. We found some similarities between tsunami generation and tsunami run-up, probably due to the similar problem geometries, specifically a planar incline. The tsunami amplitude equations formulated here show that it is possible in principle to construct accurate predictive equations for other tsunami features. Therefore, it follows that approximate tsunami shape and water velocities can be predicted at time $t = t_o$ for tsunami propagation codes. Tsunami features would in essence be transferred from the model of Grilli and Watts (1999) into analytical approximations of tsunami sources. This technique reduces landslide tsunamis to an initial condition for existing tsunami propagation codes, just like tsunamis generated by coseismic displacement. This landslide tsunami source technique has recently been validated for the 1998 Papua New Guinea tsunami (Tappin *et al.*, 2001; Watts *et al.*, 2002) and has been developed into a tsunami community model called TOPICS.

ACKNOWLEDGMENTS

The authors wish to acknowledge Applied Fluids Engineering, Inc. for substantial and extended support of this research. Partial support for this work was provided by the FEMA under grant DR-1008-9004 made to Costas Synolakis at USC, and by the NSF under research grant CMS-0100223 made to STG at URI. The authors benefited from discussions with Fumi Imamura, Gerard Fryer, Costas Synolakis, and Dave Tappin.

APPENDIX I. REFERENCES

Assier Rzadkiewicz, S., Mariotti, C., and Heinrich, P. (1997). "Numerical simulation of submarine landslides and their hydraulic effects." *J. Wtrwy, Port, Coast, and Oc. Engrg.*, ASCE, 123(4), 149-157.

Bardet, J.-P. (1997). *Experimental Soil Mechanics*. Prentice Hall, Upper Saddle River, New Jersey.

Batchelor, G. K. (1967). *An Introduction to Fluid Dynamics*. Cambridge University Press, Cambridge, UK.

Ben-Menahem, A., and Rosenman, M. (1972). "Amplitude patterns of tsunami waves from submarine earthquakes." *J. Geophys. Res.*, 77, 3097-3128.

Buckingham, E. (1914). "On Physically Similar Systems." *Phys. Rev.*, 4, 354-376.

Dean, R. G., and Dalrymple, R. A. (1991). *Water wave mechanics for engineers and scientists*. World Scientific, Teaneck, N.J.

Dobry, R., Ladd, R. S., Yokel, F. Y., Chung, R. M., and Powell, D. (1982). *Prediction of pore water pressure buildup and liquefaction of sands during earthquakes by the cyclic strain method*. NBS Building Science Series 138, Nat. Bureau Standards, U.S., Dept. of Commerce, Washington, DC

Edgers, L., and Karlsrud, K. (1982). "Soil flows generated by submarine slides: Case studies and consequences." *Nor. Geotech. Inst. Bull.*, 143, 1-11.

Fine, I. V., Rabinovich, A. B., Kulikov, E. A., Thomson, R. E., and Bornhold, B. D. (1998). "Numerical modelling of landslide-generated tsunamis with application to the Skagway Harbor tsunami of November 3, 1994." *Proc., Tsunami Symp.*, Paris.

Goldfinger, C., Kulm, L. D., McNeill, L. C., Watts, P. (2000). "Super-scale failure of the Southern Oregon Cascadia Margin." *PAGEOPH*, 157, 1189-1226.

Grilli, S. T., Skourup, J., and Svendsen, I. A. (1989). "An efficient boundary element method for nonlinear water waves." *Engrg. Analysis with Boundary Elements*, 6(2), 97-107.

Grilli, S. T., and Svendsen, I. A. (1990). "Corner problems and global accuracy in the boundary element solution of nonlinear wave flows." *Engrg. Analysis with Boundary Elements*, 7(4), 178-195.

Grilli, S. T., and Subramanya, R. (1994). "Quasi-singular integrals in the modeling of nonlinear water waves in shallow water." *Engrg. Analysis with Boundary Elements*, 13, 181-191.

Grilli, S. T., and Subramanya, R. (1996). "Numerical modeling of wave breaking induced by fixed or moving boundaries." *Comp. Mech.*, 17, 374-391.

Grilli, S. T., Svendsen, I. A., and Subramanya, R. (1998). "Breaking criterion and characteristics for solitary waves on slopes -- Closure." *J. Wtrwy, Port, Coast, and Oc. Engrg.*, ASCE, 124(6), 333-335.

Grilli, S. T., and Watts, P. (1999). "Modeling of waves generated by a moving submerged body: Applications to underwater landslides." *Engrg. Analysis with Boundary Elements*, 23(8), 645-656.

Grilli, S. T., and Watts, P. (2001). "Modeling of tsunami generation by an underwater landslide in a 3D numerical wave tank." *Proc. of the 11th Offshore and Polar Engrg. Conf.*, ISOPE01, Stavanger, Norway, 3, 132-139.

Hammack, J. L. (1973). "A note on tsunamis: Their generation and propagation in an ocean of uniform depth." *J. Fluid Mech.*, 60, 769-799.

Hampton, M. A., Lee, H. J., and Locat, J. (1996). "Submarine landslides." *Rev. Geophys.*, 34(1), 33-59.

Harbitz, C. B. (1992). "Model simulations of tsunamis generated by the Storegga slides." *Marine Geology*, 105, 1-21.

Heinrich, P. (1992). "Nonlinear water waves generated by submarine and aerial landslides." *J. Wtrwy, Port, Coast, and Oc. Engrg.*, ASCE, 118(3), 249-266.

Imamura, F., and Imteaz, M. M. A. (1995). "Long waves in two-layers: Governing equations and numerical model." *Sci. Tsunami Hazards,* 13, 3-24.

Imamura, F., and Gica, E. C. (1996). "Numerical model for tsunami generation due to subaqueous landslide along a coast." *Sci. Tsunami Hazards*, 14, 13-28.

Iwasaki, S. (1982). "Experimental study of a tsunami generated by a horizontal motion of a sloping bottom." *Bull. Earth. Res. Inst.*, 57, 239-262.

Iwasaki, S. (1987). "On the estimation of a tsunami generated by a submarine landslide." *Proc., Int. Tsunami Symp.*, Vancouver, B.C., 134-138.

Iwasaki, S. (1997). "The wave forms and directivity of a tsunami generated by an earthquake and a landslide." *Sci. Tsunami Hazards*, 15, 23-40.

Jiang, L., and LeBlond, P. H. (1992). "The coupling of a submarine slide and the surface waves which it generates." *J. Geoph. Res.*, 97(C8), 12731-12744.

Jiang, L., and LeBlond, P. H. (1993). "Numerical modeling of an underwater Bingham plastic mudslide and the waves which it generates." *J. Geoph. Res.*, 98(C6), 10303-10317.

Jiang, L., and LeBlond, P. H. (1994). "Three-dimensional modeling of tsunami generation due to a submarine mudslide." *J. Phys. Ocean.*, 24, 559-573.

Lander, J. F. (1996). *Tsunamis affecting Alaska 1737-1996*. Publication 31, Nat. Geophysical Data Ctr., Nat. Envir. Satellite, Data, and Info. Service, Nat. Oceanic and Atmospheric Admin., U.S., Dept. of Commerce, Boulder, CO.

Lander, J. F., and Lockridge, P. A. (1989). *United States tsunamis 1890-1988*. Publication 41-2, Nat. Geophysical Data Ctr., Nat. Envir. Satellite, Data, and Info. Service, Nat. Oceanic and Atmospheric Admin., U.S., Dept. of Commerce, Boulder, CO.

Lander, J. F., Lockridge, P. A., and Kozuch, M. J. (1993). *Tsunamis affecting the west coast of the United States 1806-1992*. Publication 29, Nat. Geophysical Data Ctr., Nat. Envir. Satellite, Data, and Info. Service, Nat. Oceanic and Atmospheric Admin., U.S., Dept. of Commerce, Boulder, CO.

Lee, H. J., Schwab, W. C., Edwards, B. D., and Kayen, R. E. (1991). "Quantitative controls on submarine slope failure morphology." *Marine Geotechnology*, 10, 143-157.

Li, Y., and Raichlen, F. (1998). "Breaking criterion and characteristics for solitary waves on slopes -- Discussion." *J. Wtrwy, Port, Coast, and Oc. Engrg.*, ASCE, 124(6), 329-333.

Mei, C. C. (1983). *The applied dynamics of ocean surface waves*. World Scientific, Teaneck, N.J.

Murty, T. S. (1979). "Submarine slide-generated water waves in Kitimat Inlet, British Columbia." *J. Geoph. Res.*, 84(C12), 7777-7779.

Nayfeh, A. H., and Mook, D. T. (1979). *Nonlinear Oscillations*. Wiley-Interscience, New York, NY.

Pelinovsky, E., and Poplavsky, A. (1996). "Simplified model of tsunami generation by submarine landslide." *Phys. Chem. Earth*, 21(12), 13-17.

Prior, D. B., and Coleman, J. M. (1979). "Submarine landslides: Geometry and nomenclature." *Z. Geomorph. N. F.*, 23(4), 415-426.

Sarpkaya, T., and Isaacson, M. (1981). *Mechanics of wave forces on offshore structures*. Van Nostrand Reinhold, New York, N.Y.

Schwab, W. C., Lee, H. J., Twichell, D. C. (1993). *Submarine landslides: Selected studies in the U.S. exclusive economic zone*. Bull. 2002, U.S. Geol. Surv., U.S., Dept. of Interior, Washington, DC

Seed, H. B., Seed, R. B., Schlosser, F., Blondeau, F., and Juran, I. (1988). "The landslide at the Port of Nice on October 16, 1979." *Rep. No. UCB/EERC-88/10*, Earthquake Engineering Research Center, University of California, Berkeley, CA.

Striem, H. L., and Miloh, T. (1976). "Tsunamis induced by submarine slumpings off the coast of Israel." *Int. Hydrographic Review*, 2, 41-55.

Synolakis, C. E. (1986). "The runup of long waves," PhD thesis, California Inst. of Technol., Pasadena, CA.

Tappin, D. R., Watts, P., McMurtry, G. M., Lafoy, Y., Matsumoto, T. (2001). The Sissano, Papua New Guinea tsunami of July 1998 -- Offshore evidence on the source mechanism. *Marine Geology*, 175, 1-23.

Tappin, D. R., and Shipboard Scientists. (1999). "Offshore surveys identify sediment slump as likely cause of devastating Papua New Guinea tsunami 1998." *Eos*, 80(30), July 27, 329.

Turner, A. K., and Schuster, R. L. (1996). *Landslides: Investigation and mitigation*. Special Report 247, Trans. Res. Board, National Academy Press, Washington, DC

Verriere, M., and Lenoir, M. (1992). "Computation of waves generated by submarine landslides." *Int. J. Num. Methods Fluids*, 14, 403-421.

Watts, P. (1997). "Water waves generated by underwater landslides," PhD thesis, California Inst. of Technol., Pasadena, CA.

Watts, P. (1998). "Wavemaker curves for tsunamis generated by underwater landslides." *J. Wtrwy, Port, Coast, and Oc. Engrg.*, ASCE, 124(3), 127-137.

Watts, P. (2000). "Tsunami features of solid block underwater landslides." *J. Wtrwy, Port, Coast, and Oc. Engrg.*, ASCE, 126(3), 144-152.

Watts, P., Imamura, F., and Grilli, S. T. (2000). "Comparing model simulations of three benchmark tsunami generation cases." *Sci. Tsunami Hazards*, 18(2), 107-124.

Watts, P., Borrero, J. C., Tappin, D. R., Bardet, J.-P., Grilli, S. T., Synolakis, C. E. (2002). "Novel simulation technique employed on the 1998 Papua New Guinea tsunami." Presented at the 1999 IUGG General Assembly in Birmingham, UK, and published by the first author at *www.appliedfluids.com/resume.html*.

Wiegel, R. L. (1955). "Laboratory studies of gravity waves generated by the movement of a submarine body." *Trans. Am. Geophys. Union*, 36(5), 759-774.

Yeh, H., Liu, P. L.-F., and Synolakis, C. E. (1996). *Long-wave runup models: Friday Harbor, USA, 12-17 Sept. 1995*. World Scientific, Singapore.

APPENDIX II. NOTATIONS

The following symbols are used in this paper:

A = Area and volume of SMF;
a_O = Initial SMF acceleration;
b = Length of SMF along incline;
C_d = Hydrodynamic drag coefficient;
C_m = Hydrodynamic added mass coefficient;
C_n = Coulomb friction coefficient;
d = Initial SMF submergence at maximum thickness;
g = Mean gravitational acceleration on earth surface;
Ha_o = Hammack number evaluated at time $t = t_O$;
K = Time constant;
R = Radius of curvature for slumps; run-up;
s = Position coordinate along incline;
S_u = Post-failure shear strength;
Sg = Submergence number;
S = Piston stroke;
s_o = Characteristic length scale of SMF motion;
SMF = Submarine mass failure;
t = Time;
T = Maximum SMF thickness perpendicular to the incline; piston period;
t_o = Characteristic time scale of SMF motion;
u_t = Slide terminal velocity;
u_{max} = Slump maximum velocity;
V = Volume;
w = Width of SMF along incline;
Δ = Difference;
ϕ = Angular position;
γ = SMF specific density;
Γ = SMF rate of extension along s;
η = Characteristic wave amplitude;
λ_o = Characteristic near-field wavelength;
ρ_b = Bulk SMF density;
ρ_o = Density of sea water;

θ	=	Angle of the incline from horizontal;
x	=	Horizontal position coordinate;

Subscripts

2D	=	Two-dimensional;
b	=	Bulk;
d	=	Drag;
eff	=	Effective;
g	=	Gauge;
m	=	Added mass;
n	=	Friction;
max	=	Maximum;
min	=	Minimum;
o	=	Ambient; characteristic; initial;
ref	=	Reference;
t	=	Terminal;

TABLE 1. Role of Deformation on Characteristic Amplitude

θ (degrees)	$\Gamma\sqrt{b_o / g}$	$\eta_{2d}/(s_o \sin\theta)$	$\Gamma\sqrt{b_o / g}$	$\eta_{2d}/(s_o \sin\theta)$	Difference (%)
(1)	(2)	(3)	(4)	(5)	(6)
5	0	0.008843	0.1476	0.008281	-6.4
15	0	0.007734	0.2544	0.007906	2.2
30	0	0.006334	0.3536	0.007457	17.7

TABLE 2. Parameters for Underwater Slide Model Problem Simulations

Case	γ	θ	d/b	d/d_{ref}	T/b	T/T_{ref}	s_o/b	η/b	η'	η'_{pred}
(1)	(2)	(3)	(4)	(5)	(6)	(7)	(8)	(9)	(10)	(11)
1	1.85	5	0.087	1.00	0.017	1.00	4.48	-0.0035	0.00884	0.00893
2	1.85	10	0.174	1.00	0.035	1.00	4.48	-0.0064	0.00828	0.00835
3	1.85	15	0.259	1.00	0.052	1.00	4.48	-0.0090	0.00773	0.00781
4	1.85	20	0.342	1.00	0.068	1.00	4.48	-0.0111	0.00723	0.00730
5	1.85	25	0.423	1.00	0.085	1.00	4.48	-0.0128	0.00675	0.00682
6	1.85	30	0.500	1.00	0.100	1.00	4.48	-0.0142	0.00633	0.00639
7	1.85	5	0.060	0.69	0.017	1.00	4.48	-0.0059	0.01522	0.01425
1	1.85	5	0.087	1.00	0.017	1.00	4.48	-0.0035	0.00884	0.00893
8	1.85	5	0.170	1.95	0.017	1.00	4.48	-0.0016	0.00399	0.00388
9	1.85	5	0.250	2.87	0.017	1.00	4.48	-0.0010	0.00257	0.00239
10	1.85	15	0.200	0.77	0.052	1.00	4.48	-0.0131	0.01131	0.01078
3	1.85	15	0.259	1.00	0.052	1.00	4.48	-0.0090	0.00773	0.00781
11	1.85	15	0.500	1.93	0.052	1.00	4.48	-0.0038	0.00324	0.00343
12	1.85	15	0.625	2.41	0.052	1.00	4.48	-0.0029	0.00246	0.00259
13	1.85	15	0.750	2.90	0.052	1.00	4.48	-0.0023	0.00198	0.00207
6	1.85	30	0.500	1.00	0.100	1.00	4.48	-0.0142	0.00633	0.00639
14	1.85	30	0.750	1.50	0.100	1.00	4.48	-0.0083	0.00372	0.00385
15	1.85	30	1.000	2.00	0.100	1.00	4.48	-0.0059	0.00265	0.00269
16	1.85	30	1.500	3.00	0.100	1.00	4.48	-0.0037	0.00167	0.00162
17	1.85	5	0.087	1.00	0.008	0.46	4.48	-0.0016	0.00407	0.00410
18	1.85	5	0.087	1.00	0.013	0.73	4.48	-0.0025	0.00643	0.00651
1	1.85	5	0.087	1.00	0.017	1.00	4.48	-0.0035	0.00884	0.00893
19	1.85	5	0.087	1.00	0.025	1.43	4.48	-0.0050	0.01278	0.01282
20	1.85	5	0.087	1.00	0.034	1.95	4.48	-0.0069	0.01759	0.01743
21	1.85	15	0.259	1.00	0.025	0.48	4.48	-0.0043	0.00367	0.00377
3	1.85	15	0.259	1.00	0.052	1.00	4.48	-0.0090	0.00773	0.00781
22	1.85	15	0.259	1.00	0.075	1.45	4.48	-0.0132	0.01136	0.01132
23	1.85	15	0.259	1.00	0.076	1.47	4.48	-0.0133	0.01150	0.01145
24	1.85	15	0.259	1.00	0.100	1.93	4.48	-0.0178	0.01537	0.01509
25	1.85	30	0.500	1.00	0.050	0.50	4.48	-0.0069	0.00306	0.00320
6	1.85	30	0.500	1.00	0.100	1.00	4.48	-0.0142	0.00633	0.00639
26	1.85	30	0.500	1.00	0.200	2.00	4.48	-0.0303	0.01353	0.01278
27	1.46	5	0.087	1.00	0.017	1.00	3.87	-0.0022	0.00643	0.00685
28	2.93	5	0.087	1.00	0.017	1.00	6.17	-0.0060	0.01109	0.00893
29	1.46	15	0.259	1.00	0.052	1.00	3.87	-0.0057	0.00567	0.00512
30	2.93	15	0.259	1.00	0.052	1.00	6.17	-0.0142	0.00890	0.00781
31	1.46	30	0.500	1.00	0.100	1.00	3.87	-0.0096	0.00496	0.00579
32	2.93	30	0.500	1.00	0.100	1.00	6.17	-0.0203	0.00660	0.00639

TABLE 3. Parameters for Underwater Slump Model Problem Simulations

Case	γ	θ	d/b	T/b	R/b	$\Delta\phi$	λ_o/b	η/b	η'	η'_{pred}
(1)	(2)	(3)	(4)	(6)	(6)	(7)	(8)	(9)	(10)	(11)
1	1.85	10	0.50	0.15	2.00	0.35	1.83	-0.0049	0.0812	0.0784
2	1.85	20	0.50	0.15	2.00	0.35	1.83	-0.0054	0.0456	0.0462
3	1.85	30	0.50	0.15	2.00	0.35	1.83	-0.0063	0.0359	0.0344
4	1.85	20	0.34	0.10	1.00	0.52	1.07	-0.0079	0.0886	0.0898
5	1.85	20	0.34	0.10	1.50	0.52	1.31	-0.0094	0.0700	0.0695
6	1.85	20	0.34	0.10	2.00	0.52	1.51	-0.0103	0.0573	0.0580
7	1.85	20	0.50	0.15	2.00	0.10	1.83	-0.0010	0.0280	0.0284
8	1.85	20	0.50	0.15	2.00	0.14	1.83	-0.0015	0.0318	0.0323
9	1.85	20	0.50	0.15	2.00	0.17	1.83	-0.0021	0.0348	0.0353
1 0	1.85	20	0.50	0.15	2.00	0.28	1.83	-0.0040	0.0421	0.0424
2	1.85	20	0.50	0.15	2.00	0.35	1.83	-0.0054	0.0456	0.0462
1 1	1.46	20	0.34	0.10	2.00	0.52	1.91	-0.0065	0.0363	0.0351
6	1.85	20	0.34	0.10	2.00	0.52	1.51	-0.0103	0.0573	0.0580
1 2	2.93	20	0.34	0.10	2.00	0.52	1.18	-0.0161	0.0897	0.0895

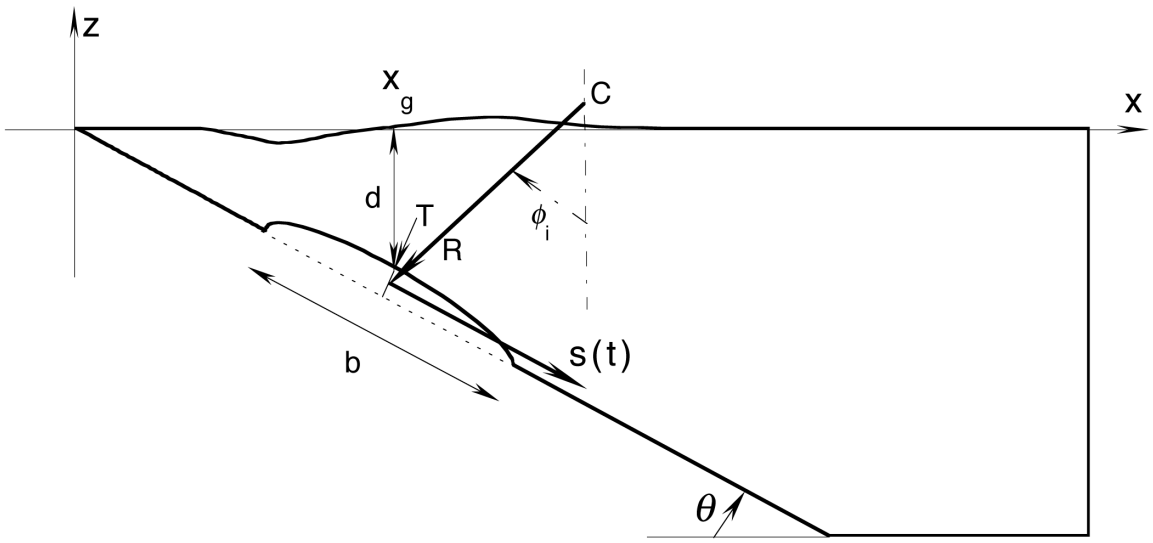

Fig. 1: Schematic diagram of model problems, for slides and slumps, with 10 fold vertical exaggeration of free surface amplitude

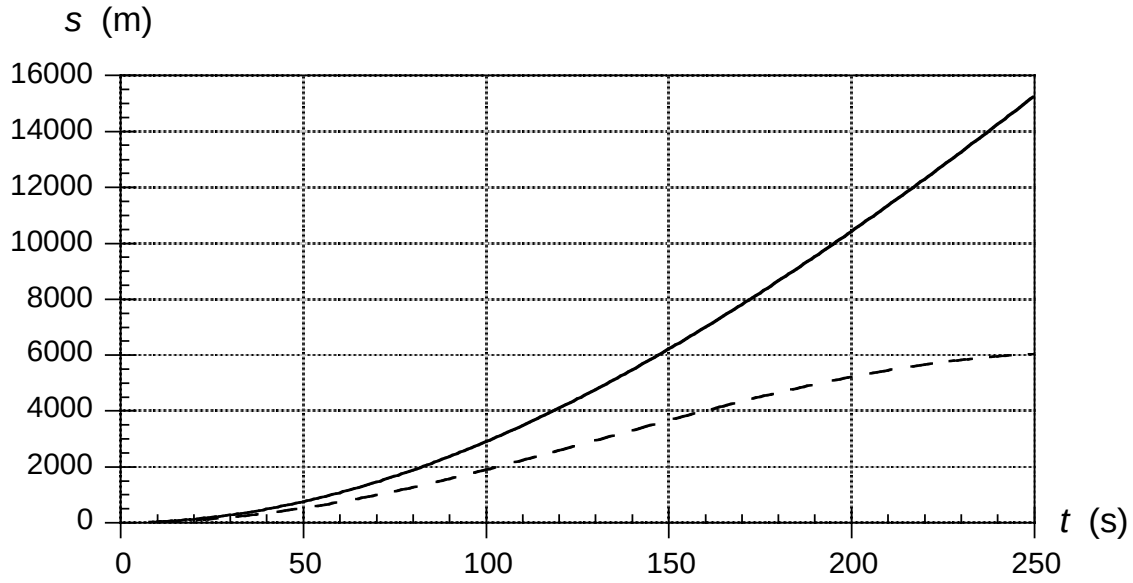

Fig. 2: Comparison of slide (———) and slump (— — —) center of mass motion

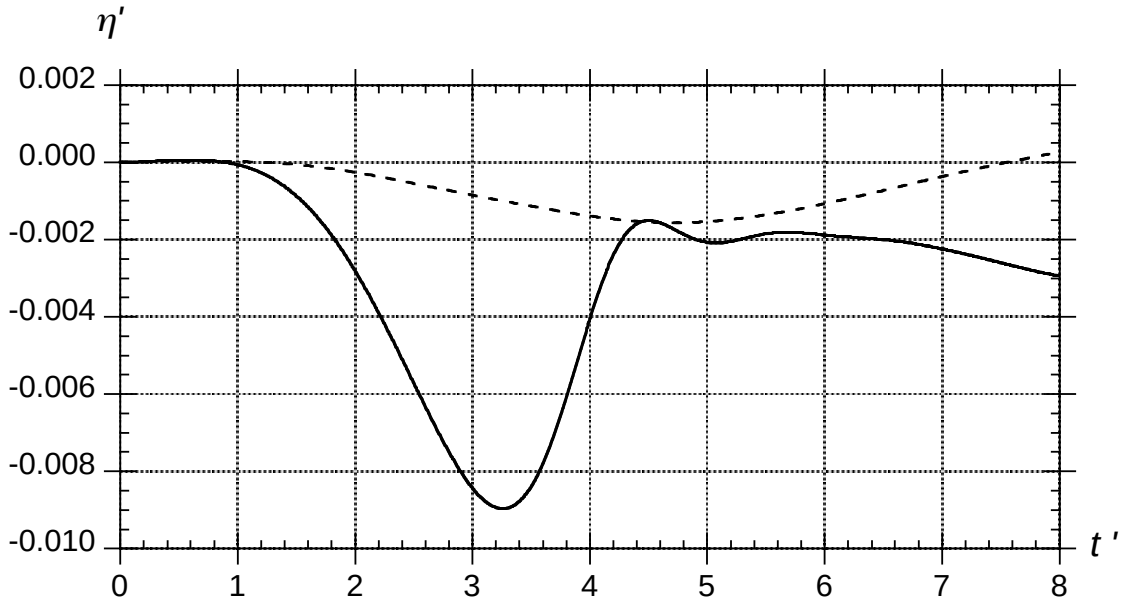

Fig. 3: Comparison of slide (———) and slump (— — —) tsunami characteristic nondimensional surface elevation $\eta' = \eta/b$, as a function of nondimensional time $t' = t(g/b)^{1/2}$

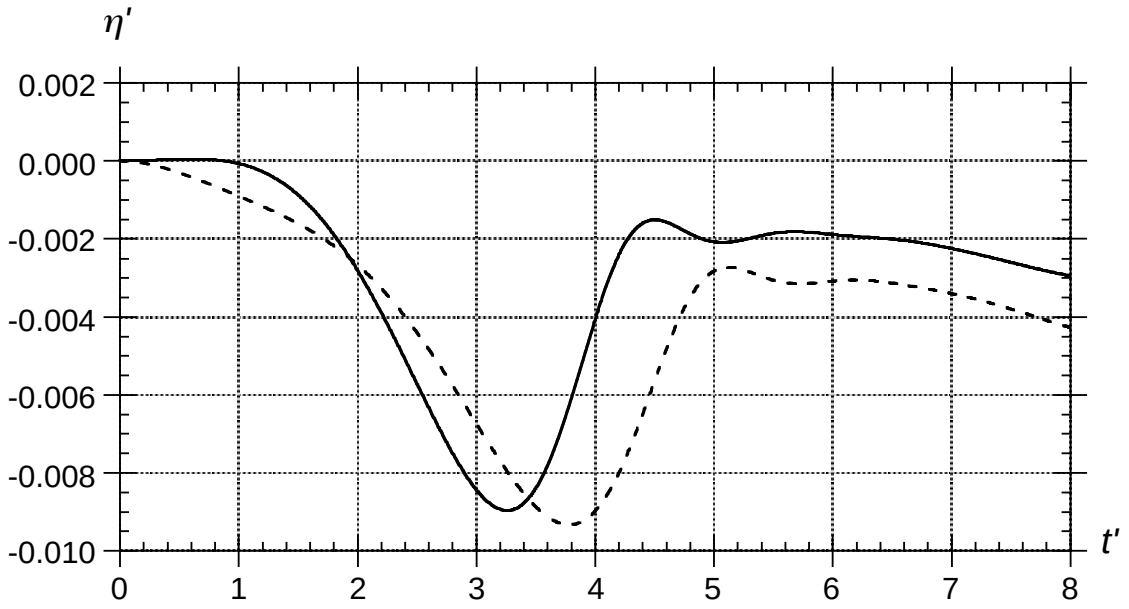

Fig. 4: Tsunami characteristic nondimensional amplitude $\eta' = \eta/(s_o \sin\theta)$ for : (———) solid; and (— — —) deforming slides, calculated as a function of nondimensional time, $t' = t(g/b)^{1/2}$.

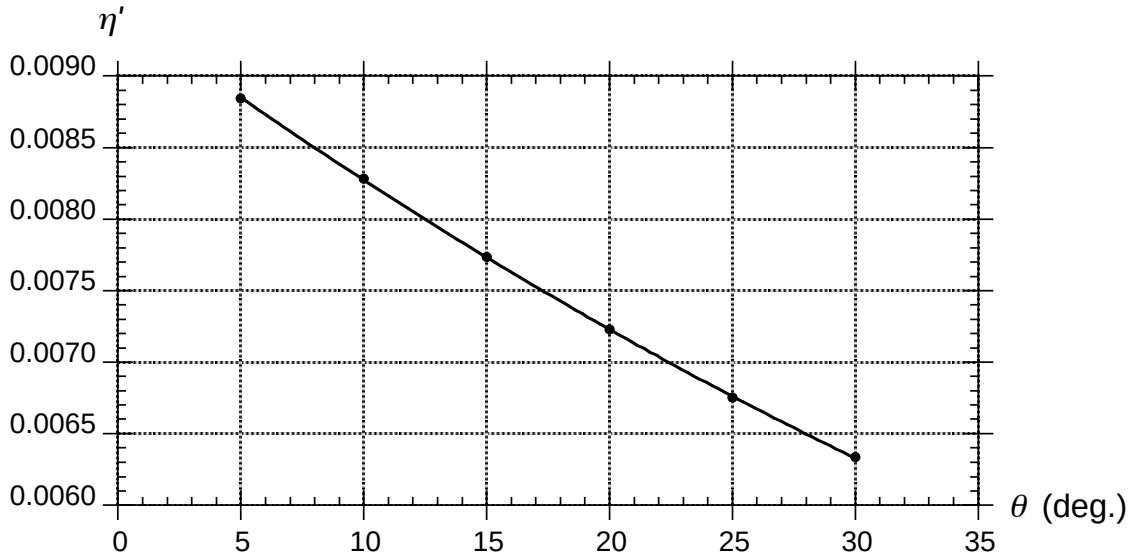

Fig. 5: Effect F of incline angle on tsunami characteristic nondimensional reference amplitude $\eta'_{ref} = \eta_{ref} / (s_o \sin\theta)$ (Eq. (20) with $T=T_{ref}$ and $d= d_{ref}$).

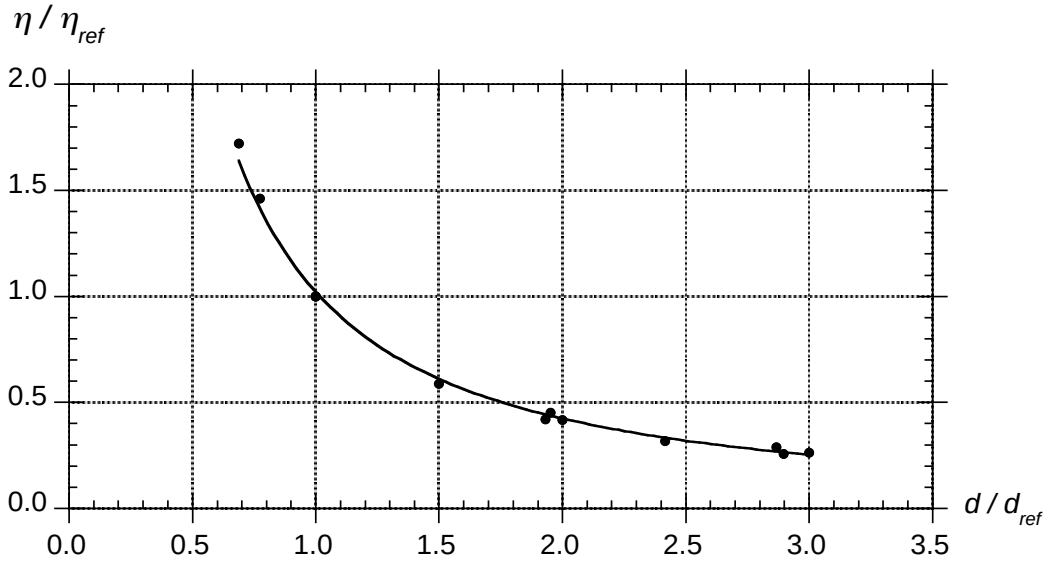

Fig. 6: Effect H of initial submergence d on tsunami characteristic amplitude η scaled by the reference value (Eq. (20) with $T = T_{ref}$).

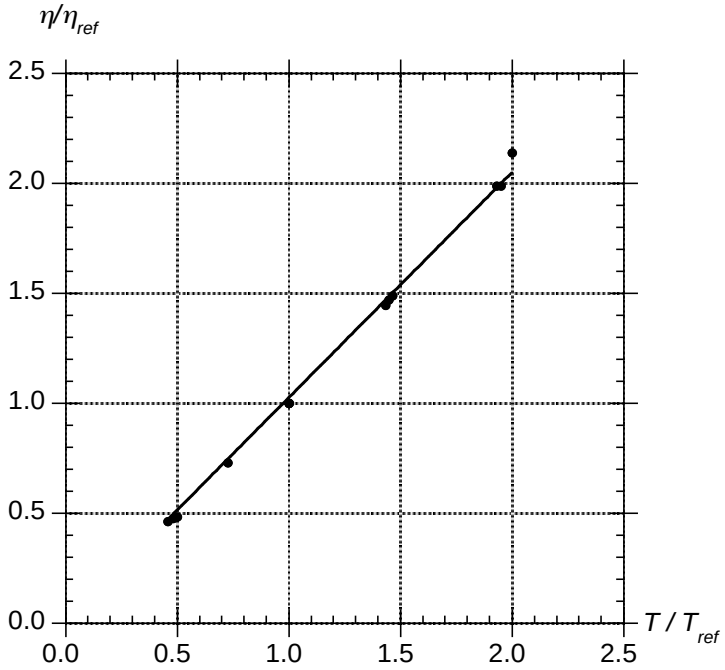

Fig. 7: Effect G of maximum thickness T on tsunami characteristic amplitude η scaled by the reference value (Eq. (20) with $d = d_{ref}$).

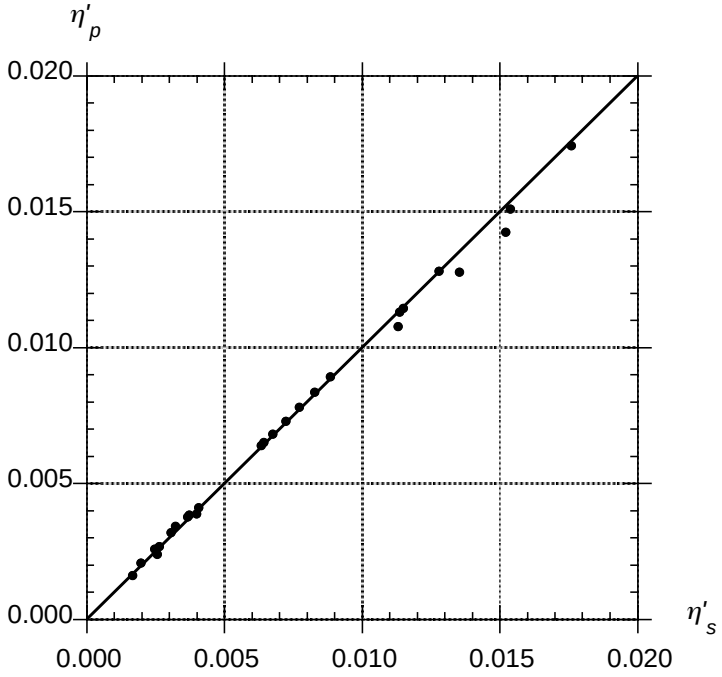

Fig. 8: Comparison of simulated (η'_s) and predicted (η'_p) nondimensional characteristic tsunami amplitudes